

Nonperturbative-transverse-momentum broadening in dihadron angular correlations in $\sqrt{s_{NN}} = 200$ GeV proton-nucleus collisions

C. Aidala,³⁹ Y. Akiba,^{50, 51, *} M. Alfred,²² V. Andrieux,³⁹ N. Apadula,²⁷ H. Asano,^{32, 50} B. Azmoun,⁷ V. Babintsev,²³ N.S. Bandara,³⁸ K.N. Barish,⁸ S. Bathe,^{5, 51} A. Bazilevsky,⁷ M. Beaumier,⁸ R. Belmont,¹² A. Berdnikov,⁵³ Y. Berdnikov,⁵³ D.S. Blau,^{31, 42} M. Boer,³⁴ J.S. Bok,⁴⁴ M.L. Brooks,³⁴ J. Bryslawskij,^{5, 8} V. Bumazhnov,²³ S. Campbell,¹³ V. Canoa Roman,⁵⁶ R. Cervantes,⁵⁶ C.Y. Chi,¹³ M. Chiu,⁷ I.J. Choi,²⁴ J.B. Choi,^{10, †} Z. Citron,⁶¹ M. Connors,^{20, 51} N. Cronin,⁵⁶ M. Csanád,¹⁶ T. Csörgő,^{17, 62} T.W. Danley,⁴⁵ M.S. Daugherty,¹ G. David,^{7, 15, 56} K. DeBlasio,⁴³ K. Dehmelt,⁵⁶ A. Denisov,²³ A. Deshpande,^{7, 51, 56} E.J. Desmond,⁷ A. Dion,⁵⁶ D. Dixit,⁵⁶ J.H. Do,⁶³ A. Drees,⁵⁶ K.A. Drees,⁶ J.M. Durham,³⁴ A. Durum,²³ A. Enokizono,^{50, 52} H. En'yo,⁵⁰ S. Esumi,⁵⁹ B. Fadem,⁴⁰ W. Fan,⁵⁶ N. Feege,⁵⁶ D.E. Fields,⁴³ M. Finger,⁹ M. Finger, Jr.,⁹ S.L. Fokin,³¹ J.E. Frantz,⁴⁵ A. Franz,⁷ A.D. Frawley,¹⁹ Y. Fukuda,⁵⁹ C. Gal,⁵⁶ P. Gallus,¹⁴ P. Garg,^{3, 56} H. Ge,⁵⁶ F. Giordano,²⁴ Y. Goto,^{50, 51} N. Grau,² S.V. Greene,⁶⁰ M. Grosse Perdekamp,²⁴ T. Gunji,¹¹ H. Guragain,²⁰ T. Hachiya,^{41, 50, 51} J.S. Haggerty,⁷ K.I. Hahn,¹⁸ H. Hamagaki,¹¹ H.F. Hamilton,¹ S.Y. Han,^{18, 50} J. Hanks,⁵⁶ S. Hasegawa,²⁸ T.O.S. Haseler,²⁰ X. He,²⁰ T.K. Hemmick,⁵⁶ J.C. Hill,²⁷ K. Hill,¹² A. Hodges,²⁰ R.S. Hollis,⁸ K. Homma,²¹ B. Hong,³⁰ T. Hoshino,²¹ N. Hotvedt,²⁷ J. Huang,⁷ S. Huang,⁶⁰ K. Imai,²⁸ M. Inaba,⁵⁹ A. Iordanova,⁸ D. Isenhower,¹ D. Ivanishchev,⁴⁹ B.V. Jacak,⁵⁶ M. Jezghani,²⁰ Z. Ji,⁵⁶ X. Jiang,³⁴ B.M. Johnson,^{7, 20} D. Jouan,⁴⁷ D.S. Jumper,²⁴ J.H. Kang,⁶³ D. Kapukchyan,⁸ S. Karthas,⁵⁶ D. Kawall,³⁸ A.V. Kazantsev,³¹ V. Khachatryan,⁵⁶ A. Khanzadeev,⁴⁹ C. Kim,^{8, 30} E.-J. Kim,¹⁰ M. Kim,^{50, 54} D. Kincses,¹⁶ E. Kistenev,⁷ J. Klatsky,¹⁹ P. Kline,⁵⁶ T. Koblesky,¹² D. Kotov,^{49, 53} S. Kudo,⁵⁹ B. Kurgyis,¹⁶ K. Kurita,⁵² Y. Kwon,⁶³ J.G. Lajoie,²⁷ A. Lebedev,²⁷ S. Lee,⁶³ S.H. Lee,^{27, 56} M.J. Leitch,³⁴ Y.H. Leung,⁵⁶ N.A. Lewis,³⁹ X. Li,³⁴ S.H. Lim,^{34, 63} M.X. Liu,³⁴ V.-R. Loggins,²⁴ S. Lökös,^{16, 17} K. Lovasz,¹⁵ D. Lynch,⁷ T. Majoros,¹⁵ Y.I. Makdisi,⁶ M. Makek,⁶⁴ V.I. Manko,³¹ E. Mannel,⁷ M. McCumber,³⁴ P.L. McGaughey,³⁴ D. McGlinchey,^{12, 34} C. McKinney,²⁴ M. Mendoza,⁸ W.J. Metzger,¹⁷ A.C. Mignerey,³⁷ D.E. Mihalik,⁵⁶ A. Milov,⁶¹ D.K. Mishra,⁴ J.T. Mitchell,⁷ I. Mitrakov,⁵³ G. Mitsuka,^{29, 50, 51} S. Miyasaka,^{50, 58} S. Mizuno,^{50, 59} P. Montuenga,²⁴ T. Moon,⁶³ D.P. Morrison,⁷ S.I. Morrow,⁶⁰ T. Murakami,^{32, 50} J. Murata,^{50, 52} K. Nagai,⁵⁸ K. Nagashima,^{21, 50} T. Nagashima,⁵² J.L. Nagle,¹² M.I. Nagy,¹⁶ I. Nakagawa,^{50, 51} K. Nakano,^{50, 58} C. Nattrass,⁵⁷ T. Niida,⁵⁹ R. Nishitani,⁴¹ R. Nouicer,^{7, 51} T. Novák,^{17, 62} N. Novitzky,⁵⁶ A.S. Nyanin,³¹ E. O'Brien,⁷ C.A. Ogilvie,²⁷ J.D. Orjuela Koop,¹² J.D. Osborn,³⁹ A. Oskarsson,³⁵ G.J. Ottino,⁴³ K. Ozawa,^{29, 59} V. Pantuev,²⁵ V. Papavassiliou,⁴⁴ J.S. Park,⁵⁴ S. Park,^{50, 54, 56} S.F. Pate,⁴⁴ M. Patel,²⁷ W. Peng,⁶⁰ D.V. Perepelitsa,^{7, 12} G.D.N. Perera,⁴⁴ D.Yu. Peressounko,³¹ C.E. PerezLara,⁵⁶ J. Perry,²⁷ R. Petti,⁷ M. Phipps,^{7, 24} C. Pinkenburg,⁷ R.P. Pisani,⁷ A. Pun,⁴⁵ M.L. Purschke,⁷ P.V. Radzevich,⁵³ K.F. Read,^{46, 57} D. Reynolds,⁵⁵ V. Riabov,^{42, 49} Y. Riabov,^{49, 53} D. Richford,⁵ T. Rinn,²⁷ S.D. Rolnick,⁸ M. Rosati,²⁷ Z. Rowan,⁵ J. Runchey,²⁷ A.S. Safonov,⁵³ T. Sakaguchi,⁷ H. Sako,²⁸ V. Samsonov,^{42, 49} M. Sarsour,²⁰ S. Sato,²⁸ B. Schaefer,⁶⁰ B.K. Schmoll,⁵⁷ K. Sedgwick,⁸ R. Seidl,^{50, 51} A. Sen,^{27, 57} R. Seto,⁸ A. Sexton,³⁷ D. Sharma,⁵⁶ I. Shein,²³ T.-A. Shibata,^{50, 58} K. Shigaki,²¹ M. Shimomura,^{27, 41} T. Shioya,⁵⁹ P. Shukla,⁴ A. Sickles,²⁴ C.L. Silva,³⁴ D. Silvermyr,³⁵ B.K. Singh,³ C.P. Singh,³ V. Singh,³ M.J. Skoby,³⁹ M. Slunečka,⁹ M. Snowball,³⁴ R.A. Soltz,³³ W.E. Sondheim,³⁴ S.P. Sorensen,⁵⁷ I.V. Sourikova,⁷ P.W. Stankus,⁴⁶ S.P. Stoll,⁷ T. Sugitate,²¹ A. Sukhanov,⁷ T. Sumita,⁵⁰ J. Sun,⁵⁶ Z. Sun,¹⁵ S. Suzuki,⁴¹ J. Sziklai,⁶² K. Tanida,^{28, 51, 54} M.J. Tannenbaum,⁷ S. Tarafdar,^{60, 61} A. Taranenko,⁴² G. Tarnai,¹⁵ R. Tieulent,^{20, 36} A. Timilsina,²⁷ T. Todoroki,^{51, 59} M. Tomášek,¹⁴ C.L. Towell,¹ R.S. Towell,¹ I. Tserruya,⁶¹ Y. Ueda,²¹ B. Ujvari,¹⁵ H.W. van Hecke,³⁴ J. Velkovska,⁶⁰ M. Virius,¹⁴ V. Vrba,^{14, 26} N. Vukman,⁶⁴ X.R. Wang,^{44, 51} Z. Wang,⁵ Y.S. Watanabe,¹¹ C.P. Wong,²⁰ C.L. Woody,⁷ C. Xu,⁴⁴ Q. Xu,⁶⁰ L. Xue,²⁰ S. Yalcin,⁵⁶ Y.L. Yamaguchi,^{51, 56} H. Yamamoto,⁵⁹ A. Yanovich,²³ J.H. Yoo,^{30, 51} I. Yoon,⁵⁴ H. Yu,^{44, 48} I.E. Yushmanov,³¹ W.A. Zajc,¹³ A. Zelenski,⁶ S. Zharko,⁵³ and L. Zou⁸

(PHENIX Collaboration)

¹Abilene Christian University, Abilene, Texas 79699, USA

²Department of Physics, Augustana University, Sioux Falls, South Dakota 57197, USA

³Department of Physics, Banaras Hindu University, Varanasi 221005, India

⁴Bhabha Atomic Research Centre, Bombay 400 085, India

⁵Baruch College, City University of New York, New York, New York, 10010 USA

⁶Collider-Accelerator Department, Brookhaven National Laboratory, Upton, New York 11973-5000, USA

⁷Physics Department, Brookhaven National Laboratory, Upton, New York 11973-5000, USA

⁸University of California-Riverside, Riverside, California 92521, USA

⁹Charles University, Ovocný trh 5, Praha 1, 116 36, Prague, Czech Republic

¹⁰Chonbuk National University, Jeonju, 561-756, Korea

¹¹Center for Nuclear Study, Graduate School of Science, University of Tokyo, 7-3-1 Hongo, Bunkyo, Tokyo 113-0033, Japan

- ¹² *University of Colorado, Boulder, Colorado 80309, USA*
- ¹³ *Columbia University, New York, New York 10027 and Nevis Laboratories, Irvington, New York 10533, USA*
- ¹⁴ *Czech Technical University, Žitkova 4, 166 36 Prague 6, Czech Republic*
- ¹⁵ *Debrecen University, H-4010 Debrecen, Egyetem tér 1, Hungary*
- ¹⁶ *ELTE, Eötvös Loránd University, H-1117 Budapest, Pázmány P. s. 1/A, Hungary*
- ¹⁷ *Eszterházy Károly University, Károly Róbert Campus, H-3200 Gyöngyös, Mátrai út 36, Hungary*
- ¹⁸ *Ewha Womans University, Seoul 120-750, Korea*
- ¹⁹ *Florida State University, Tallahassee, Florida 32306, USA*
- ²⁰ *Georgia State University, Atlanta, Georgia 30303, USA*
- ²¹ *Hiroshima University, Kagamiyama, Higashi-Hiroshima 739-8526, Japan*
- ²² *Department of Physics and Astronomy, Howard University, Washington, DC 20059, USA*
- ²³ *IHEP Protvino, State Research Center of Russian Federation, Institute for High Energy Physics, Protvino, 142281, Russia*
- ²⁴ *University of Illinois at Urbana-Champaign, Urbana, Illinois 61801, USA*
- ²⁵ *Institute for Nuclear Research of the Russian Academy of Sciences, prospekt 60-letiya Oktyabrya 7a, Moscow 117312, Russia*
- ²⁶ *Institute of Physics, Academy of Sciences of the Czech Republic, Na Slovance 2, 182 21 Prague 8, Czech Republic*
- ²⁷ *Iowa State University, Ames, Iowa 50011, USA*
- ²⁸ *Advanced Science Research Center, Japan Atomic Energy Agency, 2-4 Shirakata Shirane, Tokai-mura, Naka-gun, Ibaraki-ken 319-1195, Japan*
- ²⁹ *KEK, High Energy Accelerator Research Organization, Tsukuba, Ibaraki 305-0801, Japan*
- ³⁰ *Korea University, Seoul, 02841, Korea*
- ³¹ *National Research Center “Kurchatov Institute”, Moscow, 123098 Russia*
- ³² *Kyoto University, Kyoto 606-8502, Japan*
- ³³ *Lawrence Livermore National Laboratory, Livermore, California 94550, USA*
- ³⁴ *Los Alamos National Laboratory, Los Alamos, New Mexico 87545, USA*
- ³⁵ *Department of Physics, Lund University, Box 118, SE-221 00 Lund, Sweden*
- ³⁶ *IPNL, CNRS/IN2P3, Univ Lyon, Universit Lyon 1, F-69622, Villeurbanne, France*
- ³⁷ *University of Maryland, College Park, Maryland 20742, USA*
- ³⁸ *Department of Physics, University of Massachusetts, Amherst, Massachusetts 01003-9337, USA*
- ³⁹ *Department of Physics, University of Michigan, Ann Arbor, Michigan 48109-1040, USA*
- ⁴⁰ *Muhlenberg College, Allentown, Pennsylvania 18104-5586, USA*
- ⁴¹ *Nara Women’s University, Kita-uoya Nishi-machi Nara 630-8506, Japan*
- ⁴² *National Research Nuclear University, MEPhI, Moscow Engineering Physics Institute, Moscow, 115409, Russia*
- ⁴³ *University of New Mexico, Albuquerque, New Mexico 87131, USA*
- ⁴⁴ *New Mexico State University, Las Cruces, New Mexico 88003, USA*
- ⁴⁵ *Department of Physics and Astronomy, Ohio University, Athens, Ohio 45701, USA*
- ⁴⁶ *Oak Ridge National Laboratory, Oak Ridge, Tennessee 37831, USA*
- ⁴⁷ *IPN-Orsay, Univ. Paris-Sud, CNRS/IN2P3, Université Paris-Saclay, BP1, F-91406, Orsay, France*
- ⁴⁸ *Peking University, Beijing 100871, People’s Republic of China*
- ⁴⁹ *PNPI, Petersburg Nuclear Physics Institute, Gatchina, Leningrad region, 188300, Russia*
- ⁵⁰ *RIKEN Nishina Center for Accelerator-Based Science, Wako, Saitama 351-0198, Japan*
- ⁵¹ *RIKEN BNL Research Center, Brookhaven National Laboratory, Upton, New York 11973-5000, USA*
- ⁵² *Physics Department, Rikkyo University, 3-34-1 Nishi-Ikebukuro, Toshima, Tokyo 171-8501, Japan*
- ⁵³ *Saint Petersburg State Polytechnic University, St. Petersburg, 195251 Russia*
- ⁵⁴ *Department of Physics and Astronomy, Seoul National University, Seoul 151-742, Korea*
- ⁵⁵ *Chemistry Department, Stony Brook University, SUNY, Stony Brook, New York 11794-3400, USA*
- ⁵⁶ *Department of Physics and Astronomy, Stony Brook University, SUNY, Stony Brook, New York 11794-3800, USA*
- ⁵⁷ *University of Tennessee, Knoxville, Tennessee 37996, USA*
- ⁵⁸ *Department of Physics, Tokyo Institute of Technology, Oh-okayama, Meguro, Tokyo 152-8551, Japan*
- ⁵⁹ *Tomonaga Center for the History of the Universe, University of Tsukuba, Tsukuba, Ibaraki 305, Japan*
- ⁶⁰ *Vanderbilt University, Nashville, Tennessee 37235, USA*
- ⁶¹ *Weizmann Institute, Rehovot 76100, Israel*
- ⁶² *Institute for Particle and Nuclear Physics, Wigner Research Centre for Physics, Hungarian Academy of Sciences (Wigner RCP, RMKI) H-1525 Budapest 114, POBox 49, Budapest, Hungary*
- ⁶³ *Yonsei University, IPAP, Seoul 120-749, Korea*
- ⁶⁴ *Department of Physics, Faculty of Science, University of Zagreb, Bijenička c. 32 HR-10002 Zagreb, Croatia*

(Dated: November 19, 2021)

The PHENIX collaboration has measured high- p_T dihadron correlations in $p+p$, $p+Al$, and $p+Au$ collisions at $\sqrt{s_{NN}} = 200$ GeV. The correlations arise from inter- and intra-jet correlations and thus have sensitivity to nonperturbative effects in both the initial and final states. The distributions of p_{out} , the transverse momentum component of the associated hadron perpendicular to the trigger hadron, are sensitive to initial and final state transverse momenta. These distributions are measured multi-differentially as a function of x_E , the longitudinal momentum fraction of the associated hadron with respect to the trigger hadron. The near-side p_{out} widths, sensitive to fragmentation transverse

momentum, show no significant broadening between $p+Au$, $p+Al$, and $p+p$. The away-side nonperturbative p_{out} widths are found to be broadened in $p+Au$ when compared to $p+p$; however, there is no significant broadening in $p+Al$ compared to $p+p$ collisions. The data also suggest that the away-side p_{out} broadening is a function of N_{coll} , the number of binary nucleon-nucleon collisions, in the interaction. The potential implications of these results with regard to initial and final state transverse momentum broadening and energy loss of partons in a nucleus, among other nuclear effects, are discussed.

I. INTRODUCTION

High energy collisions of protons with nuclei provide a testing ground for quantum chromodynamics (QCD). In particular, when large transverse momentum scales are involved, the collisions can probe the quark and gluon, collectively referred to as partons, structure of the nucleus. Proton-nucleus ($p+A$) collisions have traditionally been used as a control to identify final-state nuclear effects in high energy nucleus-nucleus collisions where a strongly interacting quark-gluon plasma (QGP) is formed [1]. However, measurements in $p+A$ collisions have revealed many surprising results that have yet to be completely reconciled with each other; these have shown that understanding and explaining many different “cold” nuclear matter effects is already a challenging endeavor [2–5].

For example, in the initial-state, nuclei are known to be more complex than just a simple linear superposition of nucleons (see e.g. Ref. [2] for a review). Nuclear parton distribution functions (PDFs) are known to have several regions where they deviate from simple superpositions of nucleon PDFs as a function of the longitudinal momentum fraction x that the parton carries of the nucleon. Understanding how the partonic degrees of freedom lead to nuclear structure will be a major achievement of QCD; however, there is still significant effort required in understanding the physical origin of these measured nuclear modifications. Final-state hadronization from a nucleus can also be modified similarly to nuclear PDFs in the initial state. In particular, semi-inclusive deep-inelastic scattering (SIDIS) experiments have shown that high z hadrons are suppressed in electron-nucleus relative to electron-deuterium collisions [6], where z is the longitudinal momentum fraction of the outgoing hadron with respect to the fragmenting parton. This suppression was found to be dependent on the nuclear target size [7]. In addition, a particle species dependence was observed, which may reflect differences in the nuclear modification of quark and/or antiquark fragmentation functions and possible differences in meson versus baryon production from nuclei [6, 7].

Several proposed signatures of the QGP have also been measured in $p+A$ collisions where the overall system size created in the collision was once expected to

be too small. Collective behavior has been observed across large pseudorapidity ranges in high multiplicity $p+A$ collisions [3, 8–12]. Additionally, the enhancement of strangeness in hadron production in high multiplicity $p+A$ collisions has recently been measured [13]. Surprisingly, both of these phenomena have also been observed in high multiplicity $p+p$ collisions at Large-Hadron-Collider (LHC) energies [14, 15]. However, the suppression of high p_T inclusive hadrons or jets in $p+A$ collisions with respect to $p+p$ collisions has not been measured [16, 17]. These results were first used to establish final-state QGP interactions as the cause of high p_T hadron suppression in nucleus-nucleus collisions [5, 18]. However, the recent addition of collective and strange hadron measurements but lack of hadron suppression in $p+A$ collisions has complicated the idea that a QGP may be formed in smaller collision systems.

Another unexpected physical effect in $p+A$ collisions is the so-called “Cronin” effect, which refers to an enhancement in the inclusive hadron p_T spectrum with respect to $p+p$ collisions at moderate p_T of approximately $2 < p_T < 6$ GeV/ c which persists over a wide range of center-of-mass energies [4, 16, 19]. This effect has also been observed at moderate p_T in electron-nucleus collisions [6], where a significant dependence of the enhancement on the longitudinal momentum fraction z of the hadron was found [7]. While this was first proposed to be due to multiple scattering effects in the nuclear medium, more recent measurements have shown that hadronization also plays a role [20]. Additional measurements that go beyond single inclusive hadrons may be able to shed further light on this phenomenon in $p+A$ collisions. For example, dijet measurements in the kinematic regime of the Cronin effect have shown that the initial-state partonic transverse momentum is a function of the nucleus size [21], which has not been observed at large jet transverse momentum [22].

The lack of understanding of the underlying physical sources of these phenomena motivates measurements in new kinematic regimes with different observables. Here we present a measurement of dihadron angular correlations in $p+p$, $p+Al$, and $p+Au$ collisions at midrapidity collected by the PHENIX experiment at the Relativistic Heavy Ion Collider (RHIC). The unique capabilities of RHIC allow for a nuclear size dependence to be studied in $\sqrt{s_{NN}} = 200$ GeV $p+A$ collisions. High p_T two-particle angular correlations have been theoretically considered as a probe for energy loss in $p+A$ and $A+A$ collisions via their transverse momentum broadening [23–25]; however, the various aforementioned effects should also be consid-

* PHENIX Spokesperson: akiba@rcf.rhic.bnl.gov

† Deceased

ered as they will play a role in both collision systems. The present measurements will contribute to our understanding of the rich phenomena in hadronic interactions involving nuclei.

II. METHODS

In 2015, the PHENIX experiment [26] at RHIC collected data from $p+p$, $p+Al$, and $p+Au$ collisions at $\sqrt{s_{NN}} = 200$ GeV. A total minimum bias integrated luminosity of 60, 0.69, and 0.21 pb^{-1} for $p+p$, $p+Al$, and $p+Au$, respectively, was used for the analysis of dihadron correlations. From these total integrated luminosities, data quality assurance and collision vertex position $|z_{vtx}| < 30$ cm cuts were applied. The PHENIX detector measures two-particle angular correlations of neutral pions and charged hadrons, π^0 - h^\pm , with its electromagnetic calorimeter (EMCal) and drift chamber (DC) and pad chamber (PC) tracking system. These central arms cover an azimuthal range of $\Delta\phi \approx \pi$ radians and a pseudorapidity range of $|\eta| < 0.35$. Detailed descriptions of the PHENIX central arms can be found in Refs. [27, 28]. In $p+A$ collisions, the centrality class is determined with the forward beam-beam counters (BBCs) [29], where the centrality percentiles are defined by the multiplicity measured in the nucleus-going BBC following the procedure in Ref. [30].

The EMCal is used to identify high p_T neutral pions to construct the correlation functions. A high-energy-photon trigger is used to identify events with a high p_T photon from a $\pi^0 \rightarrow \gamma\gamma$ decay. Photons are identified using a shower shape cut that removes charged hadrons as well as most high energy clusters that overlap with another photon. The neutral pions are reconstructed via their two photon decay, where the granularity of the EMCal allows π^0 reconstruction up to approximately 20 GeV in this channel. In this analysis neutral pions are collected in the p_T range $5 < p_T < 9 \text{ GeV}/c$.

The DC and PC tracking system measures nonidentified charged hadrons in the event with the triggered high p_T photon. Two PCs, located radially behind the DC, are used to identify and match tracks in the DC with hits in the PCs. This track matching condition reduces background from secondary tracks due to conversions or decays. A ring-imaging Čerenkov system is also used to reject electrons from the charged hadron sample. With these conditions, the DC and PC tracking system is also used to reject tracks in the EMCal that happen to shower and are thus background for the $\pi^0 \rightarrow \gamma\gamma$ identification. Nonidentified charged hadrons are collected between $0.5 < p_T < 10 \text{ GeV}/c$ in correlation with the high p_T π^0 to study the correlations in as large a range as allowed by the data.

The correlations are constructed similarly to previous PHENIX two-particle correlation analyses, see e.g. Refs. [31–33]. Per-trigger yields are constructed for a given observable, such as $\Delta\phi$, which show the yield of

charged hadrons per-trigger π^0 and are defined by

$$\frac{1}{N_{\text{trig}}} \frac{dN}{d\Delta\phi} = \frac{1}{N_{\text{trig}}} \frac{dN/d\Delta\phi_{\text{raw}}}{dN/d\Delta\phi_{\text{mixed}} \epsilon(p_T)} \quad (1)$$

To account for the PHENIX acceptance, the raw correlations are divided by a mixed-event background correlation function, $dN/d\Delta\phi_{\text{mixed}}$. The background correlation is constructed with neutral pions and charged hadrons from the same data taking period but different event number; the events are required to have a similar centrality and z-vertex. To account for the efficiency of the PHENIX detector, the correlation functions are also corrected by a charged hadron efficiency defined as $\epsilon(p_T)$ in Eq. 1, which is determined with a single particle Monte Carlo generator as well as a full GEANT description of the PHENIX apparatus [34]. After these corrections, the correlations are normalized by the total number of trigger particles measured to construct the per-trigger yield and correspond to full azimuthal acceptance within $|\eta| < 0.35$.

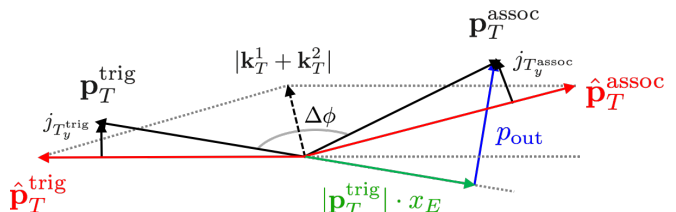


FIG. 1. A schematic diagram showing a dihadron correlation in the transverse plane. Vector quantities are shown in bold. The red vectors are the two partons, which are acoplanar due to initial-state partonic k_T , while the two black vectors are the measured trigger and associated hadron, slightly displaced from the partons due to final-state transverse momentum j_T from fragmentation. The quantities p_{out} and x_E are shown as blue and green vectors, respectively.

Correlation functions are typically constructed in terms of the azimuthal angle $\Delta\phi$ between the trigger and associated particle. Here we choose to construct the correlations as a function of the momentum space vector component p_{out} and x_E , defined as

$$p_{\text{out}} = |\mathbf{p}_T^{\text{assoc}}| \sin \Delta\phi \quad (2)$$

and

$$x_E = -\frac{\mathbf{p}_T^{\text{trig}} \cdot \mathbf{p}_T^{\text{assoc}}}{|\mathbf{p}_T^{\text{trig}}|^2} = -\frac{|\mathbf{p}_T^{\text{assoc}}|}{|\mathbf{p}_T^{\text{trig}}|} \cos \Delta\phi. \quad (3)$$

The quantities p_{out} and x_E give the transverse momentum component and longitudinal momentum fraction, respectively, of the associated hadron with respect to the trigger π^0 . These quantities are schematically diagrammed in Fig. 1, where the Figure shows a two-particle correlation in the transverse plane and quantities in bold represent vectors. In this diagram, two

hadrons (black vectors) fragment from two high p_T partons (red vectors) from a two-to-two partonic scattering. The partons are originally acoplanar due to their initial-state transverse momenta (k_T); the two hadrons may acquire additional acoplanarity due to final-state transverse momentum (j_T) during the fragmentation process. In the diagram the final-state transverse momentum is perpendicular to the parton axis and denoted as $j_{T_y}^{\text{trig}}$ and $j_{T_y}^{\text{assoc}}$, which are assumed to be Gaussian such that $\sqrt{\langle j_T^2 \rangle} = \sqrt{2\langle j_{T_y}^{\text{trig}2} \rangle} = \sqrt{2\langle j_{T_y}^{\text{assoc}2} \rangle}$. The quantity j_T could have a p_T^{trig} or p_T^{assoc} dependence to it; however, measurements have shown that this dependence is small [35]. The quantity p_{out} can be nonzero because of the k_T and j_T transverse momentum contributions, while x_E is a proxy for the momentum fraction z that the final-state hadron carries with respect to the parton; see Fig. 6 and the associated text. In the figure, x_E is shown multiplied by p_T^{trig} to explicitly show the comparison between x_E and z . When p_{out} is small, the two-particle correlation is nearly back-to-back and the acoplanarity is generated by nonperturbative k_T and j_T [33, 36]. Additional nonperturbative interactions within the nucleus, as discussed and referenced in the Introduction, may contribute to this quantity in p +A collisions.

Systematic uncertainties are assigned for the charged hadron efficiency and for the underlying event background subtraction procedure. The systematic uncertainty on the charged hadron yields is determined to be an overall normalization uncertainty of 9% on the per-trigger yields. The dominant contribution is due to the uncertainty that arises from matching tracks in the PHENIX drift chamber to the outermost pad chamber; however, there are also contributions from the overall tracking resolution of the detector and the Monte Carlo determination of the nonidentified charged hadron efficiency. The underlying event background is statistically subtracted with fits to the away-side $\Delta\phi$ correlation functions as described in Ref. [36]; these fits determine the percentage of underlying event background level with respect to the jet yield. The systematic uncertainty is determined by altering the underlying event region by $\pm 1\sigma$ based on the fit results. This uncertainty varies from less than 1% at small p_{out} to several percent at large p_{out} where the underlying event contribution, and thus background-to-signal, is larger.

III. RESULTS

Examples of the away-side per-trigger yields as a function of p_{out} are shown in several bins of x_E in Fig. 2. The per-trigger yields for p +Au and p + p collisions are shown as open and filled points, respectively. A transition from nonperturbative behavior in the nearly back-to-back $p_{\text{out}} \approx 0$ ($\Delta\phi \approx \pi$) region to perturbative next-to-leading order behavior at larger p_{out} can be seen at varying values of p_{out} , depending on the x_E bin. This change in

shape is highlighted by Gaussian fits to the small p_{out} region, drawn in Fig. 2 as dotted and solid lines for p +Au and p + p , respectively. The fit ranges vary depending on the x_E bin as the nonperturbative region is a function of p_T^{assoc} and thus x_E [33]. The fit ranges are chosen to give the best χ^2/NDF , and a systematic uncertainty is assigned based on this choice as described later; this is the dominant systematic uncertainty on the Gaussian widths. Generally the fits have a χ^2 per NDF of order ~ 10 on the p_{out} distributions when fitting only the statistical uncertainties. When fitting the systematic uncertainties, the fits always have a χ^2 per NDF less than unity. The fit results are nearly identical when fitting the statistical or systematic uncertainties; therefore, systematic uncertainties on the Gaussian widths are more conservatively estimated by adjusting the fit range when fitting to the statistical uncertainties. The fit ranges are the same for both the p + p and p +A data, and range from $[-0.4, 0.4]$ GeV/ c in the smallest x_E bin to $[-1.5, 1.5]$ GeV/ c in the largest x_E bin. These fits clearly do not describe the data at larger values of p_{out} where the data exhibit a more power-law like behavior. This transition indicates a change from sensitivity to nonperturbative to perturbative physics effects.

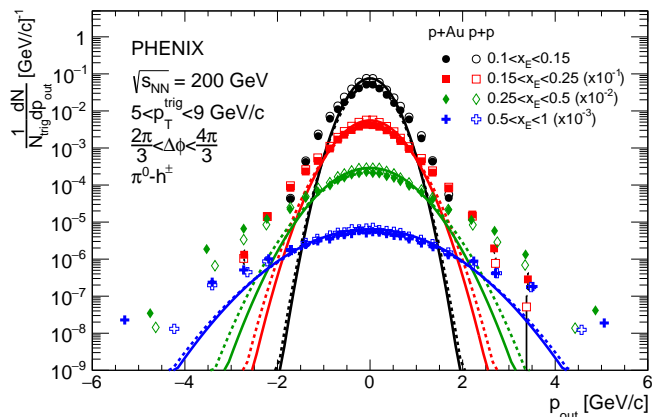


FIG. 2. The away-side p_{out} per-trigger yields are shown in both p +Au and p + p collisions for several bins of x_E . Gaussian fits, shown as dotted lines for p +Au and solid lines for p + p , are shown to the small p_{out} distributions, highlighting the nonperturbative to perturbative transition.

Examples of the near-side per-trigger yields as a function of p_{out} are shown in several bins of x_E in Fig. 3. The near-side per-trigger yields show a much narrower distribution than the away-side per-trigger yields due to the differences between intra-jet correlations and inter-jet correlations, respectively. In particular, the near-side correlations are only sensitive to fragmentation transverse momentum, because the π^0 and hadron are fragmented from the same hard parton. However, the away-side correlations are sensitive to both initial and final state transverse momentum. Because the initial-state k_T is much larger than final-state j_T (see e.g. [31, 32]), this leads to a broader p_{out} distribution on the away-side than

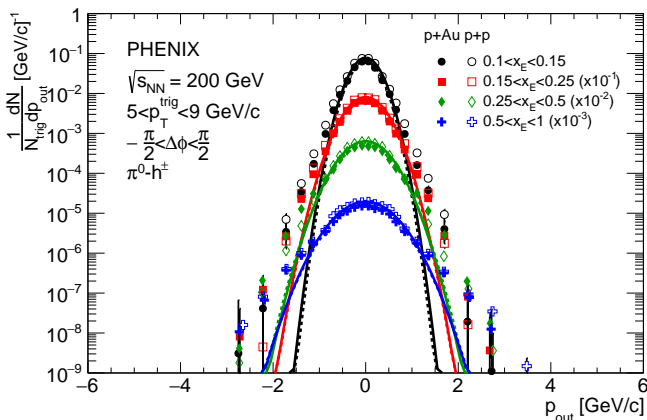


FIG. 3. The near-side p_{out} per-trigger yields are shown in both $p+\text{Au}$ and $p+p$ collisions for several bins of x_E . Gaussian fits, shown as dotted lines for $p+\text{Au}$ and solid lines for $p+p$, are performed at small p_{out} where nonperturbative behavior is dominant in the $\Delta\phi \approx 0$ region.

the near-side. Nonetheless, a nonperturbative Gaussian region can still be identified on the near side as shown in Fig. 3, similarly to the away side, with a power law spectrum at larger p_{out} that is not well described by the Gaussian fit.

To measure the nonperturbative momentum widths, the Gaussian widths are extracted from the fits to both the near and away side p_{out} distributions. Systematic uncertainties on the Gaussian widths are estimated by increasing the fit range by 0.2 GeV/c in p_{out} and taking the absolute value of the difference of the resulting Gaussian width. To study any modification in $p+A$ compared to $p+p$ collisions the squared width difference is determined between the $p+A$ and $p+p$ Gaussian widths. These differences are shown in Fig. 4 as a function of x_E for the near and away side correlation functions, for both $p+\text{Al}$ and $p+\text{Au}$ collisions. The near-side width differences in the left column of Fig. 4 show no significant modification within uncertainties between both $p+\text{Al}$ or $p+\text{Au}$ and $p+p$ collisions at all values of x_E . Similar results have been seen in dihadron correlations [35] and fragmentation function studies with full jet reconstruction [37] in $p+\text{Pb}$ collisions. However, the away-side width differences in $p+\text{Au}$ and $p+p$ collisions show modification as seen in the bottom-right panel of Fig. 4. There is no significant away-side broadening between $p+\text{Al}$ and $p+p$ collisions as seen in the top right panel of Fig. 4 within the assigned systematic uncertainties.

There is an indication that the away-side squared Gaussian width differences depend on the nucleus size as indicated in the right column of Fig. 4. To study this further, the p_{out} per-trigger yields were split into two centrality bins in the $p+\text{Au}$ data and the same analysis was performed. The centrality in $p+A$ collisions is converted to values of N_{coll} with the method in Ref. [30], where N_{coll} is defined as the average number of nucleon-nucleon collisions in a given event class. Figure 5 shows the squared

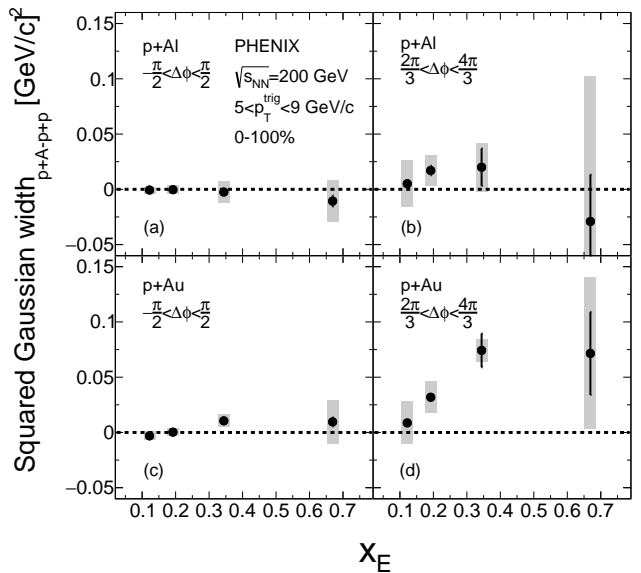


FIG. 4. The Gaussian width differences are shown for the near-side (a) and away-side (b) between $p+\text{Al}$ and $p+p$ collisions and for the near-side (c) and away-side (d) between $p+\text{Au}$ and $p+p$ collisions as a function of x_E .

width differences in $p+A$ and $p+p$ collisions as a function of N_{coll} in the two x_E bins where a nonzero Gaussian width difference is observed. The values of these squared width differences are shown in Tab. I. The data are fit with linear functions which are shown on the figure and indicate that the squared width differences exhibit a positive correlation with N_{coll} . The slopes of the fits were found to be 0.005 ± 0.001 (stat) ± 0.003 (sys) and 0.015 ± 0.005 (stat) ± 0.004 (sys) for the smaller and larger x_E bins, respectively. When the data is fit to a constant of 0, the χ^2 per number of degree of freedom becomes approximately 5 for $0.15 < x_E < 0.25$ and approximately 8 for $0.25 < x_E < 0.5$. The measured slopes differ from a slope of 0 with p values of approximately 0.055 and 0.01, for the smaller and larger x_E bins respectively, where the statistical and systematic uncertainties on the slopes were added in quadrature. This suggests that the interpretation of no transverse momentum broadening in $p+A$ compared to $p+p$ is inconsistent with the data.

IV. DISCUSSION

There are a number of different physical processes that could be contributing to the apparent broadening of the away-side nonperturbative momentum widths in $p+A$ compared to $p+p$ collisions, as discussed in the Intro-

TABLE I. The values of the Gaussian width differences between $p+A$ and $p+p$ and their statistical and systematic uncertainties are shown, corresponding to Fig. 5. Units are $[\text{GeV}/c]^2$ for the width differences and their uncertainties.

System	N_{coll}	$\sigma_{N_{\text{coll}}}$	x_E	Squared Gaussian width $_{p+A-p+p}$	(stat)	(syst)
$p+Al$	2.1	0.1	0.15–0.25	0.017	0.004	0.013
$p+Au$	4.4	0.6	0.15–0.25	0.016	0.004	0.034
$p+Au$	7.7	0.6	0.15–0.25	0.045	0.005	0.013
$p+Al$	2.1	0.1	0.25–0.50	0.020	0.017	0.022
$p+Au$	4.4	0.6	0.25–0.50	0.039	0.018	0.023
$p+Au$	7.7	0.6	0.25–0.50	0.105	0.022	0.016

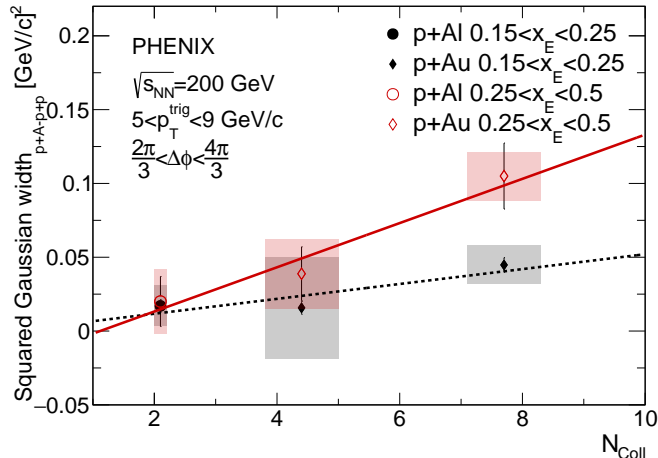


FIG. 5. The Gaussian width differences between $p+A$ and $p+p$ are shown in two x_E bins as a function of N_{coll} . Linear fits are shown for each x_E bin, which exhibit a positive dependence with N_{coll} .

duction. The apparent lack of broadening on the near-side indicates that additional nonperturbative radiation during fragmentation in $p+A$ is small. This may suggest that the fragmentation of the hard scattered parton into hadrons occurs outside any nuclear medium that is present; therefore, this fragmentation is similar between $p+A$ and $p+p$ collisions and is independent of the presence of a nucleus in the kinematic region probed by this data.

In the last decade, significant emphasis has been placed on the observation of collective effects in $p+A$ collisions. The effects of contributions from v_2 and v_3 Fourier harmonics were studied and found to be negligible in the present analysis; this is because the Gaussian widths are almost entirely constrained by correlations in the range of $\Delta\phi \pm 0.2$ radians around $\Delta\phi = \pi$. In this small $\Delta\phi$ range, any modulation from collective dynamics was found to contribute on average less than 1% to the normalization of the p_{out} correlation functions. Additionally, the correlations are collected in the midrapidity $|\eta| < 0.35$ region where the $\Delta\eta$ between the high p_T trigger and associated particle is small and thus the jet dynamics will be dominant. For this reason, any contribution from collective

dynamics can be neglected in these results.

The modification observed in this analysis is found in a similar kinematic region to where the so-called ‘‘Cronin’’ peak has been observed. In the x_E bins where the broadened widths are observed, associated hadrons corresponding to trigger neutral pions in the range $5 < p_T^{\text{trig}} < 9 \text{ GeV}/c$ are approximately in the range $1 < p_T^{\text{assoc}} < 2.5 \text{ GeV}/c$. The Cronin effect was once attributed to multiple scattering of partons within a nuclear medium; however, recent measurements revealed a particle ID dependence and have shown that additional final-state effects must also be present [20]. Additional nonperturbative initial-state partonic k_T can also contribute to the Cronin peak, to which this measurement is sensitive. Nonetheless, multiple scattering interactions within the nucleus could manifest themselves as collisional energy loss or elastic scatterings leading to an angular broadening, both of which could lead to the observed away-side momentum width broadening in $p+A$ collisions. Two-particle correlations may provide additional constraints on the underlying physical mechanism which leads to this phenomenon. Future measurements with particle identification will play an important role in identifying the cause of the Cronin peak, as a particle species dependence has been measured in $d+Au$ [20] collisions.

In Ref. [7] a strong dependence on z to the inclusive charged hadron enhancement in $e+A$ collisions was found. In particular, the largest enhancement was found for $0.2 < z < 0.4$ hadrons. Figure 6 shows the correlation between x_E and z for π^0 -hadron correlations in $\sqrt{s} = 200 \text{ GeV}$ $p+p$ collisions as determined in a PYTHIA6 [38] simulation with the default tune. The correlations are determined in the Monte Carlo simulation in the same kinematic regime as the data to draw a better comparison between z and x_E to this analysis. Figure 6 shows that $0.25 < x_E < 0.5$, where the transverse momentum broadening is observed to be the largest, corresponds approximately to a range of z covering $0.07 < z < 0.2$. This is in a similar region to where Ref. [7] sees the largest inclusive hadron enhancement in $e+A$ collisions. However, it should also be considered that the two measurements cover a much different Q^2 range, which may also be relevant in this comparison.

Nuclear PDFs can also play a role; in particular the nuclear PDFs are known to vary with the longitudinal

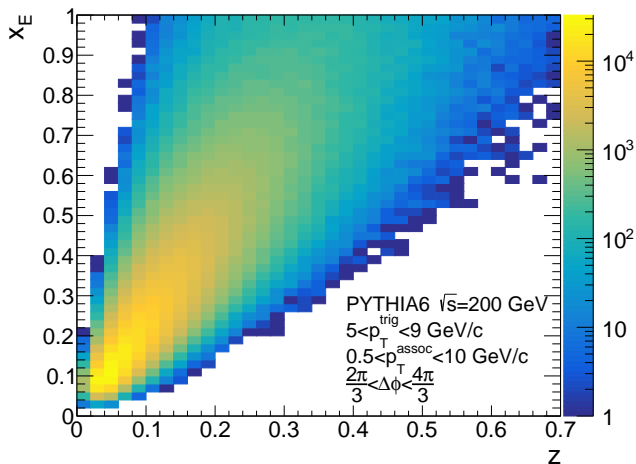


FIG. 6. The correlation between x_E and z is shown as determined in a PYTHIA simulation for π^0 -hadron correlations in the same kinematic regime as measured in the data. The correlation may provide insight into the origins of the inclusive hadron enhancement at moderate p_T in $p+A$ collisions.

momentum fraction of the parton probed [2, 39]. These measurements are in a kinematic region that may be sensitive to the anti-shadowing region around $x \approx 0.1$. The p_{out} correlation functions are also sensitive to a small transverse momentum scale, and thus can also probe the transverse-momentum-dependent parton distribution functions of the nucleus. Dijet measurements, where the jets have an average $p_T > 4$ GeV/ c , have shown that there is a larger $\Delta\phi$ acoplanarity in $p+A$ compared to $p+p$ collisions [21], indicating that there is a nuclear size dependence to initial-state partonic transverse momentum in the kinematic regime where Cronin effects may be expected to be relevant. However, the observation from the present measurement that the broadening depends on N_{coll} could indicate that the broadening is not simply due to additional transverse momentum from the nucleus size.

The transverse momentum broadening may also be due to soft radiative energy loss within the nucleus. Energy loss in cold nuclear matter has been previously studied with the Drell-Yan process [40]. Transverse momentum broadening has also been measured to be nonzero in SIDIS interactions [41]. While the Drell-Yan measurement is only sensitive to initial-state partonic energy loss, the SIDIS measurement and the measurement presented here are sensitive to both initial and final state energy loss. Global analyses which utilize all of these data may provide further insight into the origins of the measured transverse momentum broadening in nuclear Drell-Yan, SIDIS, and $p+A \rightarrow$ dihadrons processes. The difference in p_{out} between $A+A$ and $p+p$ collisions has been used to estimate the energy loss per unit length within the QGP in Au+Au collisions [25]. Given that there is an observed difference in the p_{out} widths between $p+A$ and $p+p$ collisions this indicates that small energy losses have

been measured in these dihadron correlations. Calculations for energy loss in a nucleus have been performed for both RHIC and LHC energies in the dijet and direct photon-hadron channel as well as in $e+A$ collisions [42].

V. CONCLUSION

In summary, high p_T dihadron correlations have been measured in $\sqrt{s_{NN}} = 200$ GeV $p+p$, $p+Al$, and $p+Au$ collisions. The p_{out} distributions are measured on the near and away side of the trigger hadron and the distributions are fit with Gaussian functions to extract the non-perturbative transverse momentum width in each system. The widths are compared across the various collision systems to search for modifications present in the nuclear collisions. No near-side modification is observed within uncertainties in the $p+A$ collisions, indicating that intra-jet radiation effects from nuclei are small in these systems. In contrast, the away-side widths are broadened in $p+Au$ compared to $p+p$ at moderate values of x_E , while no significant modification was observed in $p+Al$ compared to $p+p$. This was observed to be a function of the centrality or N_{coll} of the $p+A$ collision, which suggests a path length dependence to the transverse momentum broadening.

A number of different physical effects may contribute to the measured transverse momentum broadening in $p+A$ collisions. In particular, contributions from long range correlations were systematically studied and found to be small. The correlations are constructed in a kinematic regime where ‘‘Cronin’’ effects are known to be large; therefore, multiple initial-state scatterings or parton recombination effects in the final state may be contributing to the broadening. The correlations are also sensitive to the partonic initial-state transverse momentum, and thus may indicate additional primordial partonic k_T in nuclei when compared to a free nucleon. However, the dependence of the broadening on N_{coll} suggests a path length dependence to hard scattered partonic energy loss, which may be due to radiative or elastic interactions with the nuclear remnants. Considering these different qualitative physics mechanisms, and the many different processes and/or observables with which they have been measured, will be an important endeavor in understanding hadronic interactions involving nuclei. Future measurements, especially at an electron-ion collider, will continue to shed light on the many physical phenomena that occur in proton-nucleus collisions.

ACKNOWLEDGMENTS

We thank the staff of the Collider-Accelerator and Physics Departments at Brookhaven National Laboratory and the staff of the other PHENIX participating institutions for their vital contributions. We acknowledge support from the Office of Nuclear Physics in the Office

of Science of the Department of Energy, the National Science Foundation, Abilene Christian University Research Council, Research Foundation of SUNY, and Dean of the College of Arts and Sciences, Vanderbilt University (U.S.A), Ministry of Education, Culture, Sports, Science, and Technology and the Japan Society for the Promotion of Science (Japan), Conselho Nacional de Desenvolvimento Científico e Tecnológico and Fundação de Amparo à Pesquisa do Estado de São Paulo (Brazil), Natural Science Foundation of China (People's Republic of China), Croatian Science Foundation and Ministry of Science and Education (Croatia), Ministry of Education, Youth and Sports (Czech Republic), Centre National de la Recherche Scientifique, Commissariat à l'Énergie Atomique, and Institut National de Physique Nucléaire et de Physique des Particules (France), Bundesministerium für Bildung und Forschung, Deutscher Akademischer Austausch Dienst, and Alexander von Humboldt Stiftung

(Germany), J. Bolyai Research Scholarship, EFOP, the New National Excellence Program (ÚNKP), NKFIH, and OTKA (Hungary), Department of Atomic Energy and Department of Science and Technology (India), Israel Science Foundation (Israel), Basic Science Research and SRC(CENuM) Programs through NRF funded by the Ministry of Education and the Ministry of Science and ICT (Korea). Physics Department, Lahore University of Management Sciences (Pakistan), Ministry of Education and Science, Russian Academy of Sciences, Federal Agency of Atomic Energy (Russia), VR and Wallenberg Foundation (Sweden), the U.S. Civilian Research and Development Foundation for the Independent States of the Former Soviet Union, the Hungarian American Enterprise Scholarship Fund, the US-Hungarian Fulbright Foundation, and the US-Israel Binational Science Foundation.

-
- [1] K. Adcox *et al.* (PHENIX Collaboration), “Formation of dense partonic matter in relativistic nucleus-nucleus collisions at RHIC: Experimental evaluation by the PHENIX collaboration,” *Nucl. Phys. A* **757**, 184 (2005).
- [2] O. Hen, G. A. Miller, E. Piasetzky, and L. B. Weinstein, “Nucleon-Nucleon Correlations, Short-lived Excitations, and the Quarks Within,” *Rev. Mod. Phys.* **89**, 045002 (2017).
- [3] S. Chatrchyan *et al.* (CMS Collaboration), “Observation of long-range near-side angular correlations in proton-lead collisions at the LHC,” *Phys. Lett. B* **718**, 795 (2013).
- [4] J. W. Cronin, H. J. Frisch, M. J. Shochet, J. P. Boymond, R. Mermod, P. A. Piroué, and R. L. Summer, “Production of hadrons with large transverse momentum at 200, 300, and 400 GeV,” *Phys. Rev. D* **11**, 3105–3123 (1975).
- [5] K. Adcox *et al.* (PHENIX Collaboration), “Suppression of hadrons with large transverse momentum in central Au+Au collisions at $\sqrt{s_{NN}} = 130$ -GeV,” *Phys. Rev. Lett.* **88**, 022301 (2002).
- [6] A. Airapetian *et al.* (HERMES Collaboration), “Quark fragmentation to π^{\pm} , π^0 , K^{\pm} , p and anti- p in the nuclear environment,” *Phys. Lett. B* **577**, 37 (2003).
- [7] A. Airapetian *et al.* (HERMES Collaboration), “Hadronization in semi-inclusive deep-inelastic scattering on nuclei,” *Nucl. Phys. B* **780**, 1 (2007).
- [8] G. Aad *et al.* (ATLAS Collaboration), “Observation of Associated Near-Side and Away-Side Long-Range Correlations in $\sqrt{s_{NN}}=5.02$ TeV Proton-Lead Collisions with the ATLAS Detector,” *Phys. Rev. Lett.* **110**, 182302 (2013).
- [9] R. Aaij *et al.* (LHCb Collaboration), “Measurements of long-range near-side angular correlations in $\sqrt{s_{NN}} = 5$ TeV proton-lead collisions in the forward region,” *Phys. Lett. B* **762**, 473 (2016).
- [10] L. Adamczyk *et al.* (STAR Collaboration), “Long-range pseudorapidity dihadron correlations in d +Au collisions at $\sqrt{s_{NN}} = 200$ GeV,” *Phys. Lett. B* **747**, 265 (2015).
- [11] C. Aidala *et al.* (PHENIX Collaboration), “Measurement of long-range angular correlations and azimuthal anisotropies in high-multiplicity p +Au collisions at $\sqrt{s_{NN}} = 200$ GeV,” *Phys. Rev. C* **95**, 034910 (2017).
- [12] C. Aidala *et al.* (PHENIX Collaboration), “Measurements of Multiparticle Correlations in $d + Au$ Collisions at 200, 62.4, 39, and 19.6 GeV and $p + Au$ Collisions at 200 GeV and Implications for Collective Behavior,” *Phys. Rev. Lett.* **120**, 062302 (2018).
- [13] J. Adam *et al.* (ALICE Collaboration), “Multi-strange baryon production in p-Pb collisions at $\sqrt{s_{NN}} = 5.02$ TeV,” *Phys. Lett. B* **758**, 389 (2016).
- [14] G. Aad *et al.* (ATLAS Collaboration), “Observation of Long-Range Elliptic Azimuthal Anisotropies in $\sqrt{s} = 13$ and 2.76 TeV pp Collisions with the ATLAS Detector,” *Phys. Rev. Lett.* **116**, 172301 (2016).
- [15] J. Adam *et al.* (ALICE Collaboration), “Enhanced production of multi-strange hadrons in high-multiplicity proton-proton collisions,” *Nature Phys.* **13**, 535 (2017).
- [16] S. S. Adler *et al.* (PHENIX Collaboration), “Absence of suppression in particle production at large transverse momentum in $\sqrt{s} = 200$ GeV d +Au collisions,” *Phys. Rev. Lett.* **91**, 072303 (2003).
- [17] G. Aad *et al.* (ATLAS Collaboration), “Centrality and rapidity dependence of inclusive jet production in $\sqrt{s_{NN}} = 5.02$ TeV proton-lead collisions with the ATLAS detector,” *Phys. Lett. B* **748**, 392 (2015).
- [18] S. Chatrchyan *et al.* (CMS Collaboration), “Observation and studies of jet quenching in PbPb collisions at nucleon-nucleon center-of-mass energy = 2.76 TeV,” *Phys. Rev. C* **84**, 024906 (2011).
- [19] G. Aad *et al.* (ATLAS Collaboration), “Transverse momentum, rapidity, and centrality dependence of inclusive charged-particle production in $\sqrt{s_{NN}} = 5.02$ TeV p +Pb collisions measured by the ATLAS experiment,” *Phys. Lett. B* **763**, 313 (2016).
- [20] A. Adare *et al.* (PHENIX Collaboration), “Spectra and ratios of identified particles in Au+Au and d +Au collisions at $\sqrt{s_{NN}} = 200$ GeV,” *Phys. Rev. C* **88**, 024906 (2013).

- [21] M. D. Corcoran *et al.* (E609 Collaboration), “Evidence for multiple scattering of high-energy partons in nuclei,” *Phys. Lett. B* **259**, 209 (1991).
- [22] J. Adam *et al.* (ALICE Collaboration), “Measurement of dijet k_T in p-Pb collisions at $\sqrt{s_{NN}}=5.02$ TeV,” *Phys. Lett. B* **746**, 385 (2015).
- [23] R. Baier, Y. L. Dokshitzer, A. H. Mueller, S. Peigne, and D. Schiff, “Radiative energy loss and p_T broadening of high-energy partons in nuclei,” *Nucl. Phys. B* **484**, 265 (1997).
- [24] R. Baier, D. Schiff, and B. G. Zakharov, “Energy loss in perturbative QCD,” *Ann. Rev. Nucl. Part. Sci.* **50**, 37 (2000).
- [25] M. J. Tannenbaum, “Measurement of \hat{q} in relativistic heavy ion collisions using di-hadron correlations,” *Phys. Lett. B* **771**, 553 (2017).
- [26] K. Adcox *et al.* (PHENIX Collaboration), “PHENIX detector overview,” *Nucl. Instrum. Methods Phys. Res., Sec. A* **499**, 469 (2003).
- [27] K. Adcox *et al.* (PHENIX Collaboration), “PHENIX central arm tracking detectors,” *Nucl. Instrum. Methods Phys. Res., Sec. A* **499**, 489 (2003).
- [28] L. Aphecetche *et al.* (PHENIX Collaboration), “PHENIX calorimeter,” *Nucl. Instrum. Methods Phys. Res., Sec. A* **499**, 521 (2003).
- [29] K. Ikematsu *et al.*, “A Start-timing detector for the collider experiment PHENIX at RHIC-BNL,” *Nucl. Instrum. Methods Phys. Res., Sec. A* **411**, 238 (1998).
- [30] A. Adare *et al.* (PHENIX Collaboration), “Centrality categorization for $R_{p(d)+A}$ in high-energy collisions,” *Phys. Rev. C* **90**, 034902 (2014).
- [31] S. S. Adler *et al.* (PHENIX Collaboration), “Jet properties from dihadron correlations in $p + p$ collisions at $\sqrt{s} = 200$ GeV,” *Phys. Rev. D* **74**, 072002 (2006).
- [32] A. Adare *et al.* (PHENIX Collaboration), “High p_T direct photon and π^0 triggered azimuthal jet correlations and measurement of k_T for isolated direct photons in $p+p$ collisions at $\sqrt{s} = 200$ GeV,” *Phys. Rev. D* **82**, 072001 (2010).
- [33] C. Aidala *et al.* (PHENIX Collaboration), “Nonperturbative transverse-momentum-dependent effects in dihadron and direct photon-hadron angular correlations in $p+p$ collisions at $\sqrt{s} = 200$ GeV,” *Phys. Rev. D* **98**, 072004 (2018).
- [34] S. S. Adler *et al.* (PHENIX Collaboration), “PHENIX on-line and off-line computing,” *Nucl. Instrum. Methods Phys. Res., Sec. A* **499**, 593 (2003).
- [35] S. Acharya *et al.* (ALICE Collaboration), “Jet fragmentation transverse momentum measurements from di-hadron correlations in $\sqrt{s} = 7$ TeV pp and $\sqrt{s_{NN}} = 5.02$ TeV p-Pb collisions,” arXiv:1811.09742.
- [36] A. Adare *et al.* (PHENIX Collaboration), “Nonperturbative-transverse-momentum effects and evolution in dihadron and direct photon-hadron angular correlations in $p+p$ collisions at $\sqrt{s}=510$ GeV,” *Phys. Rev. D* **95**, 072002 (2017).
- [37] M. Aaboud *et al.* (ATLAS Collaboration), “Measurement of jet fragmentation in 5.02 TeV proton-lead and proton-proton collisions with the ATLAS detector,” *Nucl. Phys. A* **978**, 65 (2018).
- [38] T. Sjostrand, S. Mrenna, and P. Z. Skands, “PYTHIA 6.4 Physics and Manual,” *J. High Energy Phys.* **05** (2006) 026.
- [39] D. F. Geesaman, K. Saito, and A. W. Thomas, “The nuclear EMC effect,” *Ann. Rev. Nucl. Part. Sci.* **45**, 337–390 (1995).
- [40] M. A. Vasilev *et al.* (NuSea Collaboration), “Parton energy loss limits and shadowing in Drell-Yan dimuon production,” *Phys. Rev. Lett.* **83**, 2304 (1999).
- [41] A. Airapetian *et al.* (HERMES Collaboration), “Transverse momentum broadening of hadrons produced in semi-inclusive deep-inelastic scattering on nuclei,” *Phys. Lett. B* **684**, 114 (2010).
- [42] H. Xing, Z.-B. Kang, I. Vitev, and E. Wang, “Transverse momentum imbalance of back-to-back particle production in p+A and e+A collisions,” *Phys. Rev. D* **86**, 094010 (2012).